Structural and magnetic characterization of $[Co_2MnGe/MgO]_n$ and $[Co_2MnGe/Al_2O_3]_n$ multilayers by polarized neutron reflectivity

2008 J. Phys.: Condens. Matter 20 104217

(http://iopscience.iop.org/0953-8984/20/10/104217)

J. Phys.: Condens. Matter **20** (2008) 104217 (6pp) doi:10.1088/0953-8984/20/10/104217

Structural and magnetic characterization of $[Co_2MnGe/MgO]_n$ and $[Co_2MnGe/Al_2O_3]_n$ multilayers by polarized neutron reflectivity

M Vadalá[1], A Lamperti[2], M Wolff[1,3], K Westerholt[1] and H Zabel[1]

[1] Experimentalphysik/Festkörperphysik, Ruhr-Universität Bochum, Germany
[2] Department of Physics, University of Durham, UK
[3] Institut Laue-Langevin, Grenoble, France

Received 16 July 2007, in final form 16 August 2007
Published 19 February 2008
Online at stacks.iop.org/JPhysCM/20/104217

Abstract

We have studied multilayers of the ferromagnetic Heusler half-metal Co_2MnGe with MgO and Al_2O_3 interlayers using polarized neutron reflectivity (PNR) and magnetization measurements. The magnetization profile of the Co_2MnGe layers was determined by fitting PNR curves measured in magnetic saturation at 10 K. We find in $[Co_2MnGe/Al_2O_3]_n$ a magnetization profile definitely different from the nuclear density profile with non-ferromagnetic interlayers at the top and the bottom of each Heusler layer. In contrast, the magnetization profile of the Heusler layers in $[Co_2MnGe/MgO]_n$ is found to be more similar to the chemical profile with only a small reduction of the magnetization at both interfaces.

(Some figures in this article are in colour only in the electronic version)

1. Introduction

In recent years there has been an upsurge of interest in half-metallic ferromagnets because of their potential for technological applications in the area of spin electronics (spintronics) [1, 2]. The most promising candidates for applications in spintronic devices are compounds from the group of ferromagnetic Heusler alloys. Heusler alloys are ternary intermetallic compounds with the general composition X_2YZ, where X and Y denote a transition metal element (X = Co, Ni, Fe, ...; Y = Mn, Cr, ...) and Z is a non-magnetic element (Z = Si, Ge, ...). Theoretical band structure calculations have predicted more than 30 half-metallic ferromagnets from the Heusler group up to now [3–6]. At present the most intensively studied compounds from this group are Co_2MnSi, Co_2FeSi and Co_2MnGe, the compound we use for our present investigation, because of their high ferromagnetic Curie temperatures up to 1000 K [7–10].

The theoretically predicted 100% spin polarization at the Fermi level originates from the d–d hybridization in the minority spin states of Co and Mn, resulting in a narrow gap in the minority spin band just at the Fermi level [11]. This subtle feature makes the gap very sensitive to deviations from the ideal $L2_1$ structure, e.g. by chemical disorder, symmetry breaking at surfaces or interdiffusion at interfaces [5, 6]. This is the main reason why one encounters serious difficulties in realizing the theoretically predicted 100% spin polarization in experimental thin film systems [12].

The measurement of the tunnel magnetoresistance (TMR) of magnetic tunnelling junctions (MTJ) principally allows straightforward conclusions about the magnitude of the spin polarization at the Fermi level. In Heusler based MTJs it turned out to be very difficult until quite recently to realize the huge TMR values expected for 100% spin polarization at the Fermi energy ε_F. For many years even for high quality Heusler based MTJs one only got TMR values between typically 30% and 80% [13–15], corresponding to a spin polarization P between 30% and 60% as calculated by the Julliere formula [16]. Recently, however there was a breakthrough with TMR values of up to 570% at 2 K in tunnelling junctions with Co_2MnSi electrodes and Al_2O_3 barriers [17, 18]. These encouraging results for the first time indicated the potential of Heusler alloys in real devices. The huge TMR values were obtained for epitaxial Heusler layers and only after a high temperature

Table 1. Structural parameters of the multilayers used for the present study with the experimental parameters determined from x-ray reflectivity measurements (rms = root mean square).

	Experimental thickness (nm)		Roughness (rms) (nm)	
Nominal composition	Co_2MnGe	Al_2O_3/MgO	Co_2MnGe	Al_2O_3/MgO
$[Co_2MnGe(3\ nm)/Al_2O_3(4\ nm)]_{25}$	2.7	4.1	0.3	0.3
$[Co_2MnGe(3\ nm)/Al_2O_3(9\ nm)]_{50}$	3.1	8.9	0.3	0.6
$[Co_2MnGe(4\ nm)/MgO(4\ nm)]_{15}$	4.0	4.1	0.4	0.4

annealing process of the devices, which possibly induced a large spin polarization at the Al_2O_3/Heusler interfaces. Recently TMR values of 200% at room temperature for fully epitaxial Heusler MTJs with MgO barriers were also reported [19].

In MTJs the spin polarization of the first few monolayers close to the barrier is essential for the amplitude of the TMR. It is thus important to apply methods for a direct depth resolved analysis of the magnetism of the Heusler alloys close to interfaces. We previously have successfully accomplished this task using element specific resonant x-ray magnetic reflectivity for $[Co_2MnGe/Au]_n$ and $[Co_2MnGe/V]_n$ multilayers [20, 21] with the main result that typically 2–4 monolayers of the Heusler phase at the interfaces are non-ferromagnetic. Information about the depth dependent magnetization profile of thin ferromagnetic layers can also be deduced from an analysis of small angle neutron reflectivity using spin polarized neutrons (PNR) [22]. In the present paper we study PNR for $[Co_2MnGe/Al_2O_3]_n$ and $[Co_2MnGe/MgO]_n$ multilayers with the aim of determining the magnetization profile inside the Heusler layers.

2. Preparation and experimental procedure

The multilayers $[Co_2MnGe/Al_2O_3]_n$ and $[Co_2MnGe/MgO]_n$ were prepared in a UHV magnetron sputtering system with a base pressure of 2×10^{-9} mbar. The multilayers were deposited on a sapphire a-plane, using Ar at a pressure of 5×10^{-3} mbar as the sputter gas. The substrate temperature during deposition was 300 °C, this preparation temperature reflecting a compromise between the structural quality of the multilayers, which degrades at higher temperatures, and the value of the ferromagnetic saturation moment, which increases for higher preparation temperatures [23]. The sputter targets were prepared using stoichiometric Co_2MnGe, MgO and Al_2O_3 platelets. The sputtering rate was 0.02 nm s^{-1}, 0.01 nm s^{-1} and 0.012 nm s^{-1} for Co_2MnGe, Al_2O_3 and MgO, respectively.

The magnetization measurements were made using a Quantum Design MPMS-XL 5T SQUID magnetometer. For the standard x-ray characterization we used a conventional two-circle reflectometer with Cu Kα radiation. Polarized neutron reflectivity (PNR) measurements have been performed at the Institute Laue-Langevin (ILL, Grenoble) using the ADAM reflectometer [24]. We used cold neutrons with wavelength $\lambda = 0.441$ nm, which were polarized and analysed using transmission supermirrors. The polarization axis and the applied field direction are parallel to the sample surface and perpendicular to the scattering plane. The PNR geometry

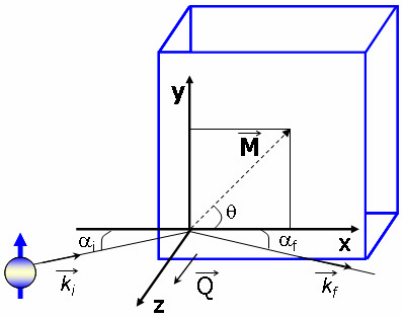

Figure 1. Scattering geometry of the PNR technique: x is the spin-flip axis, y is the non-spin-flip axis and the quantization axis for the neutrons. The magnetization vector $\vec{M}$ lies in the film plane and makes an angle θ against the x-axis. α_i, α_f are the incident and exit angles for specular reflection; the wavevectors $\vec{k}_{i,f}$ define the scattering vector $\vec{Q}$ parallel to the z-axis.

(figure 1) is such that the y-axis defines the in-plane direction parallel to the spin polarization and the x-axis defines the direction perpendicular to the spin polarization and parallel to the scattering plane. The y-axis is referred to as the non-spin-flip (NSF) axis and the x-axis as the spin-flip (SF) axis.

3. Results and discussion

3.1. Structural properties

Computer simulations of the neutron reflectivity curves revealed that in order to obtain a high sensitivity to details of the magnetization profile at the interfaces, the Heusler layers should be thin and the bilayer thickness should be larger than 10 nm. A combination of 3 nm for the Heusler layer and 9 nm for MgO or Al_2O_3 should be about right. However, whereas for the case of $[Co_2MnGe/Al_2O_3]_n$ high quality multilayers with sharp interfaces can be grown for a large thickness range of the Al_2O_3 layers, this is not possible with MgO interlayers. For $[Co_2MnGe/MgO]_n$ the roughness of the multilayer strongly increases for MgO or Co_2MnGe layer thicknesses larger than 4 nm and for the number of double-layer periods larger than 15. Thus our analysis on this system is limited to smaller double-layer thicknesses and $n = 15$.

In table 1 we summarize the structural parameters of the three multilayers which we have investigated during the present study.

In figure 2 we have depicted the small angle x-ray reflectivity as measured for the two multilayers $[Co_2MnGe(4\ nm)/Al_2O_3(3\ nm)]_{25}$ and $[Co_2MnGe(4\ nm)/MgO(4\ nm)]_{15}$ in direct comparison and together with theoretical curves calculated

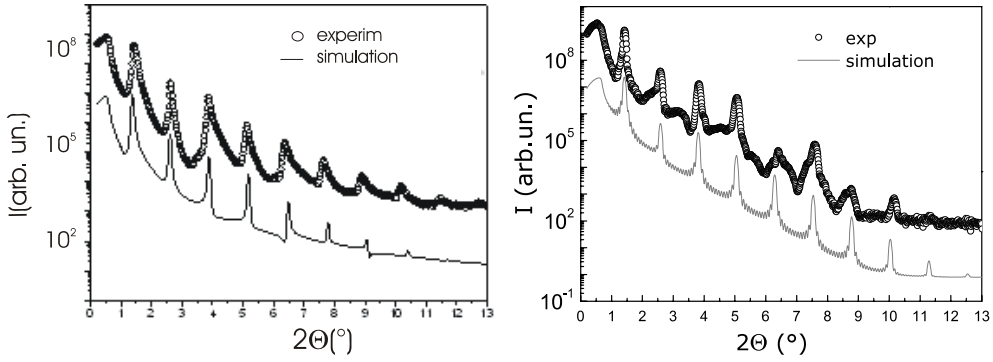

Figure 2. X-ray reflectivity for the multilayer $[Co_2MnGe(3\ nm)/Al_2O_3(4\ nm)]_{25}$ (left panel) and $[Co_2MnGe(4\ nm)/MgO(4\ nm)]_{15}$ (right panel). The solid lines are simulation results with the parameters given in table 1. The experimental curves are offset from the simulation for clarity.

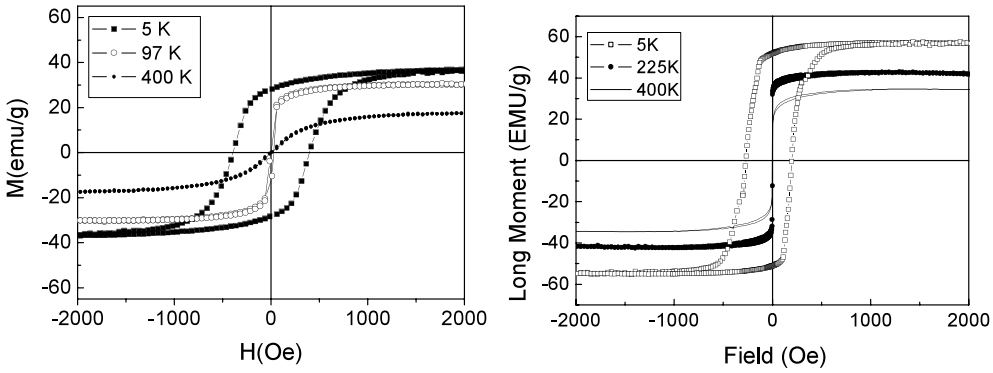

Figure 3. Magnetic hysteresis loops for the multilayer $[Co_2MnGe(3\ nm)/Al_2O_3(4\ nm)]_{25}$ (left panel) and $[Co_2MnGe(4\ nm)/MgO(4\ nm)]_{15}$ (right panel) at different temperatures.

using the Parratt formalism [25]. One can recognize superlattice reflections up to the 10th order, demonstrating a smooth layer structure with sharp interfaces. The structural parameters resulting from the theoretical fit are summarized in table 1. We also have taken x-ray Bragg scans in the range of high angles. For the multilayers with Al_2O_3 interlayers we could not resolve any Bragg reflection, indicating polycrystalline growth of the Heusler layers with a very small grain size. For the multilayer with MgO interlayers we observed a broad, weak (220)/(111) Bragg reflection, indicating a growth with (110)/(111) texture for the Heusler and MgO layers respectively.

3.2. Magnetic properties

In figure 3 we show examples of magnetic hysteresis loops for a multilayer with Al_2O_3 interlayers and MgO interlayers in direct comparison. The saturation magnetization M_s of the Heusler films at low temperatures is definitely smaller for Al_2O_3 interlayers than for MgO interlayers. The $[Co_2MnGe(3\ nm)/Al_2O_3(4\ nm)]_{25}$ multilayer saturates at about 36% of the bulk value ($M_{sbulk} = 110$ emu g^{-1} [26]), whereas the $[Co_2MnGe(4\ nm)/MgO(4\ nm)]_{15}$ multilayer reaches about 50% of the bulk M_s value. The main difference between the two systems, however, concerns the shape of the hysteresis loops observed at higher temperatures. The multilayer with MgO interlayers exhibits nearly rectangular ferromagnetic hysteresis loops with very small coercive forces up to the highest experimental temperature of 400 K, as expected for the soft ferromagnetic Heusler material. In the multilayer with Al_2O_3 interlayers, in contrast, the shape of the hysteresis loop changes drastically with increasing temperatures. The magnetization curve is completely reversible above about 100 K and the remanent magnetization vanishes here. This is a characteristic feature of superparamagnetic small particles [27] and we have observed previously a similar behaviour at high temperatures for $[Co_2MnGe/V]_n$ multilayers [28]. The temperature dependence of the remanent magnetization for all three samples of table 1 is shown in figure 4. The temperature of the vanishing remanent magnetization at about 120 K defines the blocking temperature of the superparamagnetic particles, or, more precisely, since we are dealing with interacting ferromagnetic particles, the ferromagnetic cluster glass transition temperature T_G [28].

The concept of superparamagnetic scaling [27] of the magnetization curves above T_G allows an estimation of the size of the magnetic clusters which behave superparamagnetically above T_G.

Neglecting the interaction between the clusters and assuming one single cluster size with a temperature independent cluster magnetic moment, the magnetization

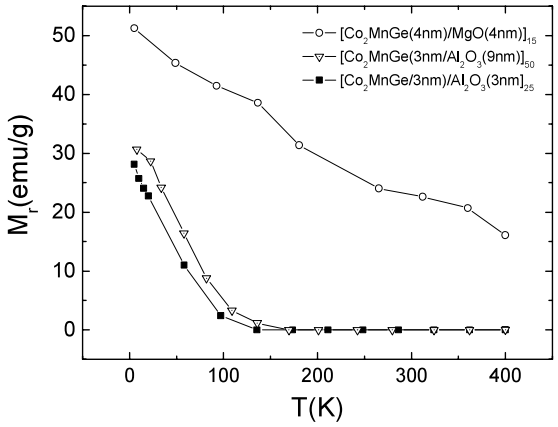

Figure 4. Remanent magnetization versus temperature for the three samples listed in table 1.

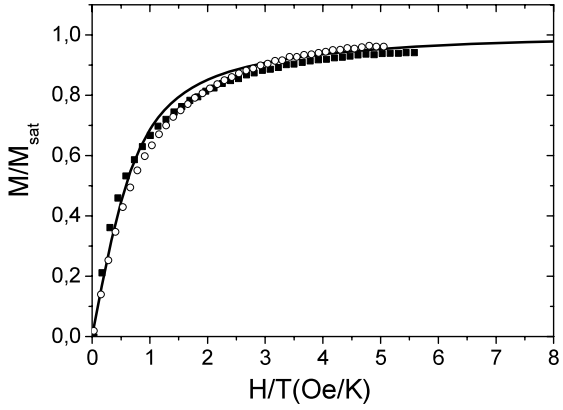

Figure 5. Scaled magnetization curves for the multilayer $[Co_2MnGe(3\ nm)/Al_2O_3(4\ nm)]_{25}$ at 400 K (open circles) and 360 K (filled squares) with a fitted curve (drawn line) corresponding to the Langevin function with the cluster moment of $\mu_c = 3 \times 10^4\ \mu_B$ (see the main text).

above T_g should scale as

$$M(H,T) = N_c \mu_c L\left(\frac{\mu_c H}{k_B T}\right)$$

with the number of magnetic clusters N_c, the cluster magnetic moment μ_c and the Langevin function $L(x)$.

The experimental curves above room temperature can be reasonably well approximated by this scaling function, if one takes the temperature dependence of the saturation magnetization of Co_2MnGe into account. In figure 5 we show one example for the $[Co_2MnGe(3\ nm)/Al_2O_3(4\ nm)]_{25}$ multilayer. From the fit of the Langevin function in figure 5 we derive a cluster magnetic moment of $\mu_c = 3 \times 10^4\ \mu_B$, which corresponds to the magnetization of about 1.5×10^4 Co_2MnGe formula units or to an average lateral cluster size of about 16×16 nm^2 within each Co_2MnGe layer. Below room temperature the magnetization curves can still be approximated by a Langevin function, however with definite deviations from the scaling function in figure 5 towards a larger initial slope, suggesting that the magnetic clusters increase in size with decreasing temperature or the interactions between the clusters become of growing importance.

Microscopically the magnetic clusters and the superparamagnetic behaviour originate from a magnetic decoupling at large angle grain boundaries of the polycrystalline grains within each Co_2MnGe layer. Disorder of Heusler alloys at grain boundaries leads to a vanishing ferromagnetic order and to a strong weakening of the magnetic coupling between the grains [23].

3.3. Polarized neutron reflectivity

In figure 6 we have plotted the specular non-spin-flip R^+ and R^- reflectivity curves (the $+$ and $-$ signs defining the spin directions parallel and antiparallel to the guiding field) for the $[Co_2MnGe(3\ nm)/Al_2O_3(9\ nm)]_{50}$ and the $[Co_2MnGe(4\ nm)/MgO(4\ nm)]_{15}$ multilayers. The data in figure 6 were recorded at 10 K in a magnetic field 1000 Oe, i.e. large enough to magnetically saturate the Heusler layers. The ferromagnetic splitting of the R^+ and R^- reflectivity clearly shows up, especially at the Bragg peak positions. For the multilayer with the Al_2O_3 interlayers (left panel of figure 6) one immediately notes an interesting feature, namely a crossover of the scattering intensity in the R^+ and the R^- channel beyond the third-order Bragg peak, with the intensity for R^+ being larger than that for R^- for higher scattering angles. Since the magnetic and nuclear scattering lengths have the same sign for R^+ and the opposite sign for R^-, this is only possible if the magnetization profile is different from the nuclear density profile and asymmetric with respect to the growth direction.

The neutron reflectivity data in figure 6 were simulated using the structural data from the fitting of the x-ray reflectivity in table 1 and allowing the formation of reduced or non-ferromagnetic interlayers in the magnetization profile at the top and bottom interfaces with different widths d_t and d_b. The thickness of the reduced ferromagnetic interlayers and the magnetic scattering length density are the fitting parameters in the simulation. The simulations were performed using the super-iterative routine generalizing the conventional Parratt formalism to the reflection of spin 1/2 particles from a multilayer with n double layers [29].

The best fit to the $[Co_2MnGe/Al_2O_3]_{50}$ multilayer was achieved by assuming reduced ferromagnetic interlayers with a thickness of $d_t = 0.5$ and $d_b = 1.2$ nm for the top and the bottom of the Heusler layers, respectively, or vice versa (see figure 7). From the neutron reflectivity data we cannot determine whether the top or the bottom has the thicker non-ferromagnetic layer. However, it is reasonable to assume that when growing Heusler films on an amorphous interlayer, full order and increase of magnetization requires a certain thickness which is bigger than at the top, where order is destroyed by the deposition of the next amorphous aluminium oxide layer. Thus we observed an asymmetric magnetization profile perpendicular to the film, as mentioned above. From the magnetic scattering length we calculate a magnetic moment of 1.46 μ_B per Co_2MnGe formula unit, in good agreement with the magnetization measurements.

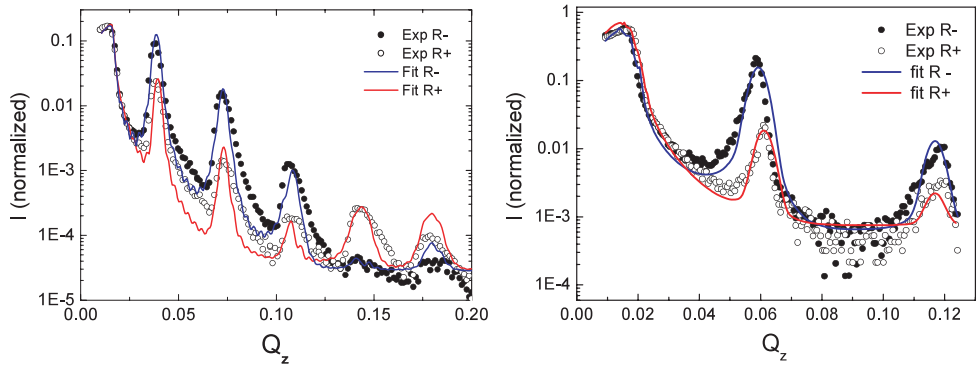

Figure 6. Specular non-spin-flip reflectivity R^- (full dots) and R^+ (open dots) taken at 10 K and 1000 Oe for the multilayer $[Co_2MnGe(3\ nm)/Al_2O_3(9\ nm)]_{50}$ (left panel) and $[Co_2MnGe(4\ nm)/MgO(4\ nm)]_{15}$ (right panel). The solid lines are theoretical fits (see the main text).

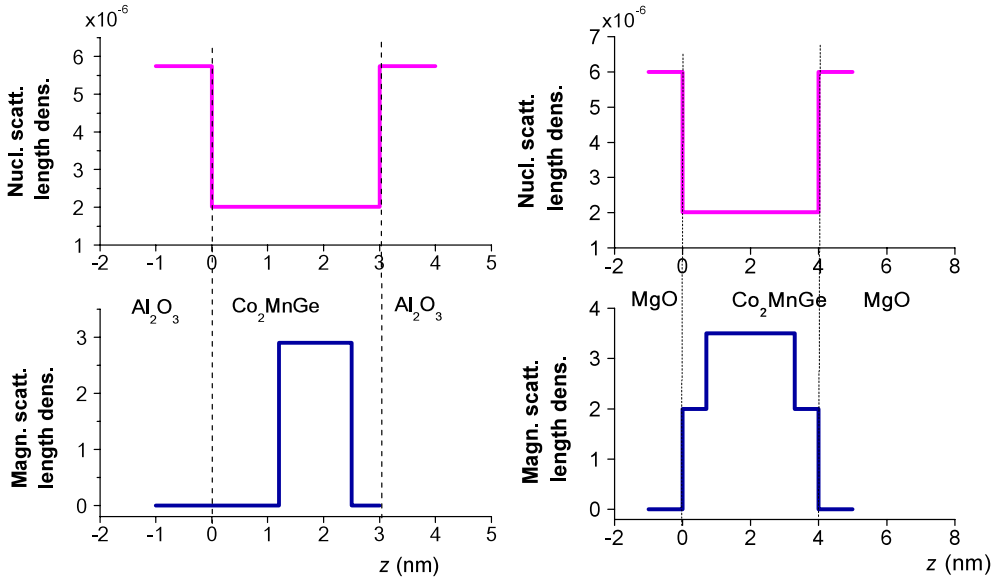

Figure 7. Nuclear and magnetic scattering length density as a function of the z-direction perpendicular to the film plane for the multilayer $[Co_2MnGe(3\ nm)/Al_2O_3(4\ nm)]_{25}$ (right panel) and for $[Co_2MnGe(4\ nm)/MgO(4\ nm)]_{15}$ (left panel). We clearly observe an asymmetric profile for the multilayer $[Co_2MnGe(3\ nm)/Al_2O_3(4\ nm)]_{25}$.

For the $[Co_2MnGe/MgO]_{15}$ multilayer the best fit was obtained assuming a magnetization profile with the magnetization dropping to about 60% of the core value at both interfaces, for an interlayer thickness of 0.6 nm (see figure 7). From the magnetic scattering length density determined in the fit we calculate a magnetic moment of 2.8 μ_B per Co_2MnGe formula unit, which is also in good agreement with the bulk magnetization measurements.

Off-specular neutron scattering gives additional information about the in-plane structure of the interfaces and their correlations. Two-dimensional reflectivity maps recorded at 10 K in magnetic saturation are depicted in figure 8 for two multilayers with Al_2O_3 and MgO interlayers. The spots along the diagonal ridge $\alpha_i = \alpha_f$ correspond to the Bragg peaks of figure 6. For both multilayers we do not observe Bragg sheets in the direction perpendicular to the specular Bragg spots. Thus correlated magnetic or structural roughness can be excluded. Simultaneously the intensity of the diffuse scattering into the off-specular reciprocal space is weak, indicating sharp interfaces with negligible interdiffusion and uncorrelated small magnetic clusters.

4. Summary and conclusions

Our study of the multilayers $[Co_2MnGe/Al_2O_3]_n$ and $[Co_2MnGe/MgO]_n$ revealed that the interfaces between the oxide and the Heusler phase are smooth in both systems with negligible interdiffusion, both features being prerequisites for a good performance of magnetic tunnelling junctions. The quality of the ferromagnetism of the Heusler layers is much better for the case of $[Co_2MnGe/MgO]_n$ than for $[Co_2MnGe/Al_2O_3]_n$, i.e. the saturation magnetization is larger and the multilayer is ferromagnetic up to the highest experimental temperature of 400 K. The superparamagnetism above 100 K and the non-ferromagnetic interlayers characterizing $[Co_2MnGe/Al_2O_3]_n$ are absent in

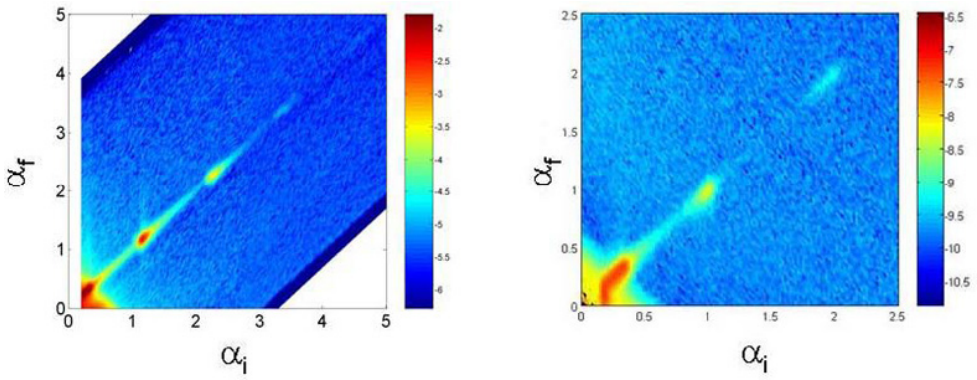

Figure 8. PNR intensity R^+ map of $[Co_2MnGe(4\ nm)/Al_2O_3(9\ nm)]_{25}$ (left figure) and R^+ map of $[Co_2MnGe(4\ nm)/MgO(4\ nm)]_{15}$ (right figure) recorded at 10 K in a field of 1000 Oe.

$[Co_2MnGe/MgO]_n$. The reason for this different behaviour is probably a different growth mode of the Heusler phase on the MgO and Al_2O_3 surface. On amorphous Al_2O_3 the Heusler phase grows in a disordered fashion with very small, polycrystalline grains. On the crystalline MgO surface the growth is more ordered and textured. There is a rather good lattice matching between Co_2MnGe and MgO with a lattice mismatch of only about 3%, which favours the growth of an ordered Heusler phase.

From the results presented here we conclude that for MTJs with Heusler electrodes the use of MgO as the barrier material should be a much better choice. However, the fabrication of high quality, pinhole free and very thin MgO barriers on Co_2MnGe is another onerous and challenging task.

Acknowledgments

The authors would like to acknowledge Professor B P Toperverg for providing the fitting program. The financial support provided through the European Union's Marie Curie actions (Research Training Networks) ULTRASMOOTH under contract MRTN-CT-2003-504462, the DFG (SFB 491), and BMBF (03ZA6BC1) are gratefully acknowledged.

References

[1] Prinz G 1998 *Science* **282** 1660
[2] Awschalom D and Kikkawa J 1999 *Phys. Today* **52** 33
[3] de Groot R A, Muller F M, van Engen P G and Buschow K H J 1983 *Phys. Rev. Lett.* **50** 2024
[4] Ishida S, Kashiwagi S, Fujii S and Asano S 1995 *Physica* B **210** 140
[5] Galanakis I, Dederichs P H and Papanikolaou N 2002 *Phys. Rev.* B **66** 134428
[6] Picozzi S, Continenza A and Freeman A J 2004 *Phys. Rev.* B **69** 094423
[7] Kallmayer M, Elmers H J, Balke B, Wurmehl S, Emmerling F, Fecher G H and Felser C 2006 *J. Phys. D: Appl. Phys.* **39** 096402
[8] Hashemifar S J, Kratzer P and Scheffler M 2005 *Phys. Rev. Lett.* **90** 096402
[9] Kämmerer S, Heitmann S, Meyners D, Sudfeld D, Thomas A, Hütten A and Reiss G 2003 *J. Appl. Phys.* **93** 7945
[10] Okamura S, Miyazaki A, Sugimoto S, Tezuka N and Inomata K 2005 *Appl. Phys. Lett.* **86** 232503
[11] Galanakis J and Dederichs P H 2005 *Half-Metallic Alloys—Fundamentals and Applications* (*Springer Lecture Notes Phys.* vol 667) ed P H Dederichs and J Galanakis (Berlin: Springer) p 1
[12] Wang W H, Przybylski M, Kuch W, Chelaru L I, Wang J, Lu Y F, Barthel J, Meyerheim H L and Kirschner J 2005 *Phys. Rev.* B **71** 144416
[13] Tanaka C, Novak J and Moodera J S 1997 *J. Appl. Phys.* **81** 5515
Tanaka C, Novak J and Moodera J S 1999 *J. Appl. Phys.* **86** 6230
[14] Schmalhorst J, Kämmerer S, Sacher M, Reiss M, Hütten A and Scholl A 2004 *Phys. Rev. Lett.* **70** 024426
[15] Verduijn E and Westerholt K 2006 *J. Appl. Phys.* **99** 084502
[16] Julliere M 1975 *Phys. Lett.* A **54** 225
[17] Sakuraba Y, Nakata J, Oogane M, Kubota H, Ando Y, Sakuma A and Miyazaki T 2005 *Japan. J. Appl. Phys.* **44** L1100
[18] Sakuraba Y, Hattori M, Oogane M, Ando Y, Kato H, Sakuma A and Miyazaki T 2006 *Appl. Phys. Lett.* **88** 192508
[19] Tezuka N, Ikeda N, Sugimoto S and Inomata K 2006 *Appl. Phys. Lett.* **89** 252508
[20] Grabis J, Bergmann A, Nefedov A, Westerholt K and Zabel H 2005 *Phys. Rev.* B **72** 024438
[21] Bergmann A, Nefedov A, Westerholt K and Zabel H 2006 *J. Phys. D: Appl. Phys.* **39** 842
[22] Majkrzak C F, O'Donovan K V and Berk N F 2006 *Neutron Scattering from Magnetic Materials* ed T Chatterji (Amsterdam: Elsevier)
[23] Westerholt K, Bergmann A, Grabis J, Nefedov A and Zabel H 2005 *Half-Metallic Alloys—Fundamentals and Applications* (*Springer Lecture Notes Phys.* vol 667) ed P H Dederichs and J Galanakis (Berlin: Springer) p 67
[24] Scheyer A, Siebrecht R, English U, Pietsch U and Zabel H 1999 *Physica* B **355** 267–8
[25] Parratt L G 1954 *Phys. Rev.* B **95** 359
[26] Ziebeck P J and Webster K R A 1988 *Landolt–Börnstein New Series 1, Group III* vol 19c (Berlin: Springer)
[27] Altbir D, Kiwi M, Ramırez R and Schuller I K 1995 *J. Magn. Magn. Mater.* **149** L246
[28] Bergmann A, Grabis J, Leiner V, Wolff M, Zabel H and Westerholt K 2005 *Phys. Rev.* B **72** 214403
[29] Toperverg B P 2004 *Polarized Neutron Scattering* (*Series Matter and Materials* vol 12) ed Th Brückel and W Schweika (Jülich: Forschungszentrum Jülich) p 247